PAPER • OPEN ACCESS

Gadolinium-chelate functionalized magnetic CuFeSe$_2$ ternary nanocrystals for T1-T2 dual MRI and CT imaging *in vitro* and *in vivo*

To cite this article: Lu-Yao Lai *et al* 2021 *Mater. Res. Express* **8** 045001

View the article online for updates and enhancements.

Materials Research Express

PAPER

Gadolinium-chelate functionalized magnetic CuFeSe$_2$ ternary nanocrystals for T1-T2 dual MRI and CT imaging *in vitro* and *in vivo*

Lu-Yao Lai[1,5], **Ying Jiang**[2,5], **Guang-Ping Su**[1], **Min Wu**[3], **Xiao-Fei Lu**[1], **Shao-Zhi Fu**[4], **Lu Yang**[1,*] **and Jian Shu**[1,*]

1   Department of Radiology, The Affiliated Hospital of Southwest Medical University, Luzhou, Sichuan, People's Republic of China
2   Department of Radiology, The 2nd Affiliated Hospital of Chengdu Medical College Nuclear Industry 416 Hospital, Chengdu, Sichuan, People's Republic of China
3   Department of Radiology, Chongqing Traditional Chinese Medicine Hospital, Chongqing, People's Republic of China
4   Department of oncology, The Affiliated Hospital of Southwest Medical University, Luzhou, Sichuan, People's Republic of China
5   These authors contributed to the work equally and should be regarded as co-first authors.
*   Authors to whom any correspondence should be addressed.

E-mail: yangluchem@qq.com and shujiannc@163.com

Abstract

CuFeSe$_2$ nanomaterial with high thermal conversion efficiency, well superparamagnetism, effective x-ray attenuation ability, multifunctional groups and excellent biocompatibility is beneficial to the construction of multimodal imaging probes which can combine various imaging modes to provide a synergistic advantage over a single imaging mode. This study aimed to develop a novel multimodal nanocontrast agent CuFeSe$_2$@diethylenetriaminepentaacetic acid (DTPA)-Gd to obtain imaging information with high specificity, high sensitivity and high contrast. The morphology and physical characteristics of CuFeSe$_2$@DTPA-Gd were detected by transmission electron microscope, scanning electron microscope, x-ray single crystal diffraction, vibrating sample magnetometer and fourier transform infrared spectrometer. The toxicity of CuFeSe$_2$@DTPA-Gd *in vivo* was evaluated by hematoxylin-eosin staining. The imaging capability of CuFeSe$_2$@DTPA-Gd *in vitro* and *in vivo* was evaluated by magnetic resonance imaging (MRI) and computed tomography (CT). This study successfully prepared nanoparticles CuFeSe$_2$@DTPA-Gd, and experimental results in this study demonstrated CuFeSe$_2$@DTPA-Gd is expected to be a useful CT and MRI T1-weighted imaging/T2-weighted imaging three-modal contrast agent in clinic.

1. Introduction

Malignant tumors extremely endanger the health and quality of patients' life. Meanwhile, patients' death is closely related to late diagnosis at an advanced stage and difficulty of treatment. So, early detection, diagnosis and treatment are critical to the therapeutic schedule, prognosis of tumors and the quality of patients' life [1–4]. Pathological examination is the gold standard for tumor diagnosis. As an invasive examination method, its procedures are difficult to follow and results are always influenced by the location of sampling. For these reasons, it is restricted to the early diagnosis and detection of tumor progression. It's still difficult for conventional noninvasive imaging methods that including ultrasound imaging, magnetic resonance imaging (MRI), computed tomography (CT) imaging and radionuclide imaging, etc to detect tumors early and make accurate diagnosis of tumor location and classification [5–7]. With the rapid development and continuous application of nanotechnology and molecular probes, imaging diagnosis is gradually deepened from traditional anatomical imaging to molecular imaging which is non-invasive, real-time, accurate, and highly specific because of detailed information of cell and molecule [8–10]. Not only advanced imaging equipment, novel and efficient imaging probes are also factors that promote the development of molecular imaging. Currently, traditional non-specific

contrast agents, nanoprobes and molecular probes with specific molecular ligands are commonly used [11, 12]. Nanoparticles refer to a class of materials with a one-dimensional space size <100 nm, which can be comparable to the size of large biomolecules, such as enzymes, receptors, and antibodies, etc. In addition, They are able to accumulate and remain stable in tumor tissues by the enhanced permeability-retention effect, nanoparticles is a material with relatively larger ratio of superficial area to volume which makes it have the ability to target multiple binding sites by being loaded with a variety of components [13–16]. This indicates that nanoparticles can provide higher binding efficiency to target specific tumor sites.

By some operations such as surface modification and signal component assembly of nanomaterials, we can get nanoprobes with imaging function. Common types of nanoprobes include MRI, CT, radionuclide imaging, optical imaging, and photoacoustic imaging probes, etc. However, the single model imaging method has its own advantages and limitations, here are some examples: optical imaging has the advantages of no radiation, real-time imaging, short imaging time, etc, but also has disadvantages such as weak penetrating power, interference of autofluorescence, etc; CT has strong penetration ability, high spatial resolution, short imaging time and other advantages, but it has a certain radiation to the human body and its resolution to soft tissues is relatively low; Although MRI has the advantages of multi-directional, multi-sequence, multi-parameter imaging, high soft tissue resolution, no radiation, etc, its sensitivity is relatively weak and imaging time is long; Radionuclide imaging has high sensitivity and can provide functional information of tissues or organs, but its specificity is insufficient, and there may be some false positive and false negative results. If we can combine two or even multiple imaging methods to achieve multimodal imaging which can provide complementary information among multiple imaging methods and collaborative advantage, we may obtain the highly specific functional imaging information and high sensitivity, high contrast anatomical imaging information. The development of multimodal probes that combine various imaging modes with their own imaging advantages while maintaining their size advantages, well biocompatibility and targeting will be one of the main challenges of multimodal imaging [17]. As multimodal probes need relatively more groups to realize multimodal imaging, nanomaterials with large surface areas are just such a good carrier to provide many binding sites [11, 18, 19]. As in the previous research by Liang *et al* Gd and gold nanoclusters were successfully coupled to form a fluorescence-magnetic resonance dual-modality imaging probe [20]. Of course, it will be of great significance for the development of diagnostic and therapeutic modalities if nanometer contrast agent that can integrate multimodal imaging and have precise therapeutic capabilities can be synthesized for cancer theranostics [21].

The multimodal nanometer contrast agent $CuFeSe_2$ used in this study is a ternary sulfide nanomaterial. At present, most of the studies on magnetic trichalcogenides nanostructures have focused on Cu-Fe-S and Cu-CO-S nanocrystals, with little attention paid to Cu-Fe-Se nanostructures (such as $CuFeSe_2$). $CuFeSe_2$ nanocrystals have high photothermal conversion efficiency (82%), superparamagnetic properties and effective x-ray attenuation, as well as excellent water solubility, colloidal stability, biocompatibility and multifunctional groups, making them ideal nanoprobes for multimodal imaging and tumor photothermal therapy [22]. Currently, $CuFeSe_2$ is mainly prepared by hot solution injection, solvothermal method, pyrochemical process, etc, not only the production process is complex, but also the products are easy to lose the advantages of small size and there are problems of water solubility and biocompatibility [23, 24].

Therefore, this study environment friendly prepared $CuFeSe_2$ coupled DTPA in the water phase, and obtained multi-functional nanometer contrast agent $CuFeSe_2$@DTPA-Gd which was designed specifically for CT and MRI T1-weighted imaging (T1WI)/T2-weighted imaging (T2WI) three-mode imaging and be uniform morphology, well solubility, high biocompatibility, and low toxicity. Meanwhile, its imaging capabilities *in vitro and in vivo*, and toxicity *in vivo* were tested in this study.

2. Material and methods

2.1. Materials and instruments

Selenium powder (Se), sodium borohydride ($NaBH_4$), Copper (II) chloride dihydrate ($CuCl_2 \cdot 2H_2O$), Ferrous sulfate heptahydrate ($FeSO_4 \cdot 7H_2O$), DTPA, Gadolinium chloride hexahydrate ($GdCl_3 \cdot 6H_2O$) were purchased from Sigma-Aldrich (USA). Cell culture materials were purchased from Beyotime, Gibco and Biological Industries.

The size and morphology of the synthesized $CuFeSe_2$, $CuFeSe_2$@DTPA and $CuFeSe_2$@DTPA-Gd were characterized by transmission electron microscope (TEM) (JEM1200-EX, JEOL Ltd, Japan). The hydrodynamic size was determined by Dynamic Light Scattering Particle Sizing Analyzer (NanoBrook 90Plus Zeta, Brookhaven Instruments Corporation, USA) at 25 °C. The morphology and elemental composition of the nanoparticles were analyzed by scanning electron microscope (SU8020, Hitachi, Japan). The surface functional groups of nanoparticles were detected by infrared absorption spectra obtained by fourier transform infrared spectrometer (Nicolet IS10, Thermo fisher, America). The crystal structures of $CuFeSe_2$, $CuFeSe_2$@DTPA and

CuFeSe$_2$@DTPA-Gd were determined by x-ray single crystal diffraction (XRD) (D8 ADVANCE, Brucker, Germany). The scanning conditions were as follows: 2θ range 10°–90°, scanning rate 6° min^{-1}, and scanning step length 0.02. Magnetic properties of CuFeSe$_2$ and CuFeSe$_2$@DTPA-Gd solutions at 300 K were tested by vibrating sample magnetometer (VSM) (Versalab, Quantum Design, USA), and the magnetization isotherm was obtained.

2.2. Preparation of CuFeSe$_2$@DTPA-Gd nanocrystals
The preparation of CuFeSe$_2$ was based on the methods reported in the previous study [23], and CuFeSe$_2$@DTPA-Gd is prepared by the method described below. 39.48 mg of Se powder was dispersed in 100 ml of ultrapure water, and then 50 mg of NaBH$_4$ was added to reduce it at ambient conditions with protection of argon flow. After Se powder was completely reduced, a 5 ml mixture of CuCl$_2$·2H$_2$O (42.62 mg), FeSO$_4$·7H$_2$O (69.75 mg), and DTPA (200 mg) were added. After continued stirring overnight, CuFeSe$_2$@DTPA was obtained by centrifugal separation, and was placed in 20 ml ultrapure water after washed three times with ultrapure water and anhydrous ethanol respectively. CuFeSe$_2$@DTPA-Gd nanocrystals was obtained by centrifugation after Gadolinium chloride hexahydrate (205.36 mg) was added and stirred for 24 h. Finally, wash with ultrapure water for 3 times and store in pure water for later use.

2.3. Cell culture and cytotoxicity
Human breast cancer MCF-7 cells and Human normal breast cells MCF10A were donated by the Department of Oncology, Affiliated Hospital of Southwest Medical University. Cells were cultured in DMEM supplemented with 10% fetal bovine serum (FBS) in a cell incubator with condition of 37 °C and 5% CO$_2$ condition.

This study determined the cell survival rate by the standard MTT assay. MCF7 cells and MCF10A cells were seeded at logarithmic phase to sterile 96-well cell culture plate at 3×10^3 cells per well, respectively. Next, different concentrations of CuFeSe$_2$@DTPA-Gd (150 ug ml^{-1}, 30 ug ml^{-1}, 6 ug ml^{-1}, 1.2 ug ml^{-1} and 0.24 ug ml^{-1}) were added to the wells. The cells were then incubated for 24 h in incubator with condition of 37°C and 5% CO$_2$.

2.4. Toxicity *in vivo*
BABL/C female mice (n = 16) were divided into 4 groups and injected with 0.2 ml CuFeSe$_2$@DTPA-Gd (1.5 mg ml^{-1}) through the tail vein. The mice were sacrificed on the 1st, 3rd, 7th and 15th days respectively. The main organs (heart, liver, spleen, lung and kidney) were taken and fixed with 4% formalin. Then sliced and stained with hematoxylin-eosin (HE) staining. Above organs of untreated BABL/C female mice were used as controls (n = 4).

2.5. CT and MRI imaging *in vitro*
Various CuFeSe$_2$@DTPA-Gd concentrations (0.1 mg ml^{-1}, 0.2 mg ml^{-1}, 0.4 mg ml^{-1}, and 1.5 mg ml^{-1}) were used for measurements of CT values on a 64 row 128-slice spiral CT scanner (General Electric Company, USA) with 80 Kev tube voltages and 80 mA tube current. Each concentration is 2 ml, and 2 ml ultrapure water was used as the control.

Similarly, various CuFeSe$_2$@DTPA-Gd concentrations (0.1 mg ml^{-1}, 0.2 mg ml^{-1}, 0.4 mg ml^{-1}, 1.5 mg ml^{-1}) were used for measurements on a 3 T MR scanner (Philips, Netherlands) with a small animal coils at 25 °C. T1 relaxometry was measured with a SE sequence with a TR of 8.3 ms, a TE of 4.5 ms. The acquired images had a FOV of 160 mm × 120 mm × 30 mm, and a slice thickness of 0.7 mm. T2 relaxometry was performed using a SE sequence with a TR of 4000 ms and a TE of 128. Each concentration is 2 ml, and 2 ml ultrapure water was used as the control.

2.6. Multimodal imaging *in vivo*
The animal experiments of this study were approved by Experimental Animal Ethics Committee of Southwest Medical University. 1×10^6 MCF-7 cells in 0.2 ml saline were subcutaneously injected into 6–8 weeks female BABL/C mouse right leg root to get MCF-7 tumor model used for MRI and CT imaging. When the tumor volume reaches 100 mm^2, the model was considered successful and *in vivo* imaging was subsequently performed.

For CT imaging, each mouse was intratumorally injected with 0.2 ml 1.5 mg ml^{-1} CuFeSe$_2$@DTPA-Gd. CT imaging were performed on anesthetized mice (Intraperitoneal injection of 1% pentobarbital sodium, 0.1–0.15 ml/per mice) before and after injection of CuFeSe$_2$@DTPA-Gd with 80Kev tube voltage and 80 mA tube current (n = 4). The largest cross-section of the tumor was selected from the CT workstation, and the region of interest was sketched in the tumor area.

For MRI imaging, each mouse was intratumorally injected with 0.2 ml 1.5 mg ml^{-1} CuFeSe$_2$@DTPA-Gd. MRI T1WI and T2WI imaging were performed on anesthetized mice (Intraperitoneal injection of 1% pentobarbital sodium, 0.1–0.15 ml per mice) before and after injection of CuFeSe$_2$@DTPA-Gd (n = 4). T1 signal intensity was measured with a SE sequence with a TR of 8.3 ms, a TE of 4.5 ms. The acquired images had a FOV of 88 mm × 88 mm × 30 mm, and a slice thickness of 0.7 mm. T2 signal intensity was performed using a SE sequence with a TR of 4000 ms and a TE of 128. The largest cross-section of the tumor was selected from the MRI workstation, and the region of interest was sketched in the tumor area and the spinal erector muscle area at the same level. Tumor signal intensity before injection (SICpre), muscle signal intensity before contrast injection (SIMpre), tumor signal intensity after injection (SICpost), muscle signal intensity after contrast injection (SIMpost), and ratio of SIC to SIM were generated.

In addition, IQon Spectral CT (Philips, Netherlands) and MAGNETOM Prisma MRI (Siemens, Germany) coronal imaging were performed on another MCF-7 tumor model mouse (tumor located in the left thigh). The tumor modeling process and imaging process are the same as described above. IQon CT imaging parameters were as follows: tube voltage was 120KV, tube current was 265 mA, slice thickness was 0.8 mm. Prisma MRI imaging parameters were as follows: T2Map value was measured with a TR of 1000.0 ms, a TE of 13.8 ms, a FOV of 120 mm × 120 mm × 13 mm, and a slice thickness of 1 mm; T2*Map value was measured with a TR of 293.0 ms, a TE of 2.98 ms, a FOV of 120 mm × 120 mm × 13 mm, and a slice thickness of 1 mm.

2.7. Statistical analysis

The statistical analyses involved in this study were processed by SPSS17.0 statistical software (International Business Machines Corporation, America). SI$_C$, SI$_C$/SI$_M$ and CT values of tumor area before and after contrast agent injected were expressed as mean ± Std.Error ($\bar{X}$ ± SE). The pared-samples T test was used to compare the different SI$_C$, SI$_C$/SI$_M$ and CT values of the tumor area before and after CuFeSe$_2$@DTPA-Gd injected. The test level α = 0.05 (both sides), and P < 0.05 was considered statistically significant.
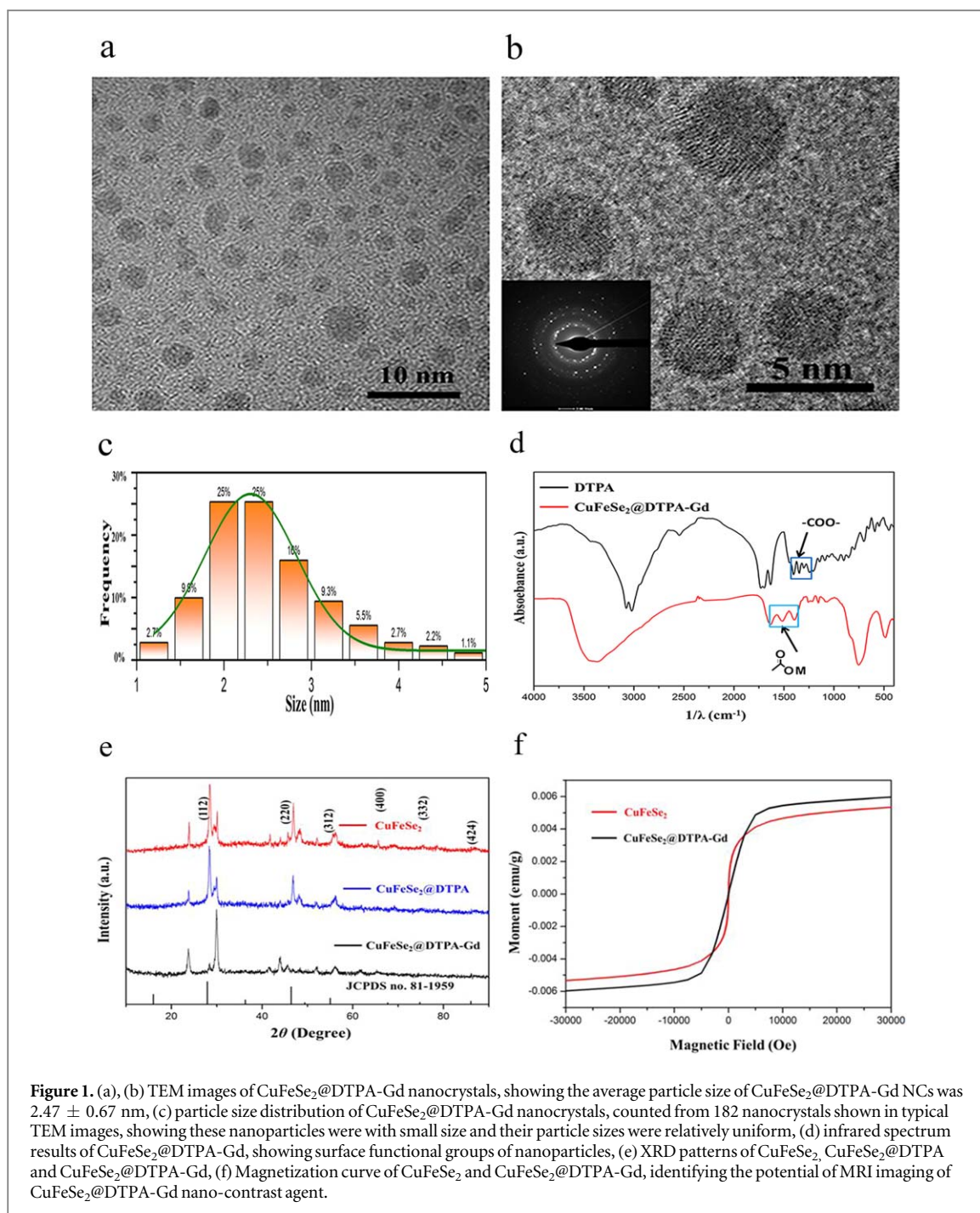
3. Results and discussion

3.1. Characterization of CuFeSe$_2$@DTPA-Gd nanocrystals

Nanoparticles are normally transferred from the blood to the reticuloendothelial system (RES) including the liver and spleen, and may lead to potential toxicity risk as most nanoparticles will accumulate in RES organs [25]. The nanoparticles with smaller size are more likely to pass through the glomerular filtration membrane and be excreted, thereby reducing the uptake of the reticuloendothelial system. The morphology and size of nanoparticles synthesized in this study were determined by TEM. The spherical nanoparticles CuFeSe$_2$@DTPA-Gd with sizes of (2.47 ± 0.67) nm were observed and their particle sizes were relatively uniform (figures 1(a)–(c)). The TEM images of CuFeSe$_2$ and CuFeSe$_2$@DTPA were shown in the supplementary figure 1 (available online at stacks.iop.org/MRX/8/045001/mmedia). The CuFeSe$_2$@DTPA-Gd synthesized in this study was relatively small in size, which is beneficial to reduce the potential risk. The results of energy spectrum analysis indicated that the CuFeSe$_2$@DTPA-Gd nanometer contrast agent contains Cu, Fe, Se and Gd elements (supplementary figure 2(a)). The Infrared spectrum results of CuFeSe$_2$@DTPA-Gd were shown in figure 1(d). The crystal structures of CuFeSe$_2$ and CuFeSe$_2$@DTPA-Gd were further characterized by XRD, and the obtained patterns were in complete agreement with the tetragonal crystal shape (CuFeSe$_2$, JCPDS no. 81-1959) (figure 1(e)).

VSM is usually used to detect the entire magnetization of magnetic nanoparticles. It can be observed through the magnetization isotherm that CuFeSe$_2$ and CuFeSe$_2$@DTPA-Gd show good superparamagnetization under the condition of K = 300 and the external magnetic field strength is in the range of −30000 ~ 30000 Oe (figure 1(f)). The well superparamagnetization of CuFeSe$_2$ and CufeSe$_2$@DTPA-Gd also indicated the MRI imaging potential of CuFeSe$_2$@DTPA-Gd nano-contrast agent. And, it can be seen from supplementary figures 2(b)–(d) that the CuFeSe$_2$@DTPA-Gd dispersed in different media (H$_2$O and 10% FBS) and over different time (0 h, 24 h and 48 h) showed similar hydrodynamic size. The above results demonstrated that CuFeSe$_2$@DTPA-Gd nanocrystals synthesized in this study could show excellent solubility and stability in H$_2$O or 10% FBS. In addition, although the hydrodynamic size of CuFeSe$_2$@DTPA-Gd dispersed in water was measured to be 285.44 nm which was different from that measured by TEM, it can be explained by different procedures and principles of DLS and TEM methods.
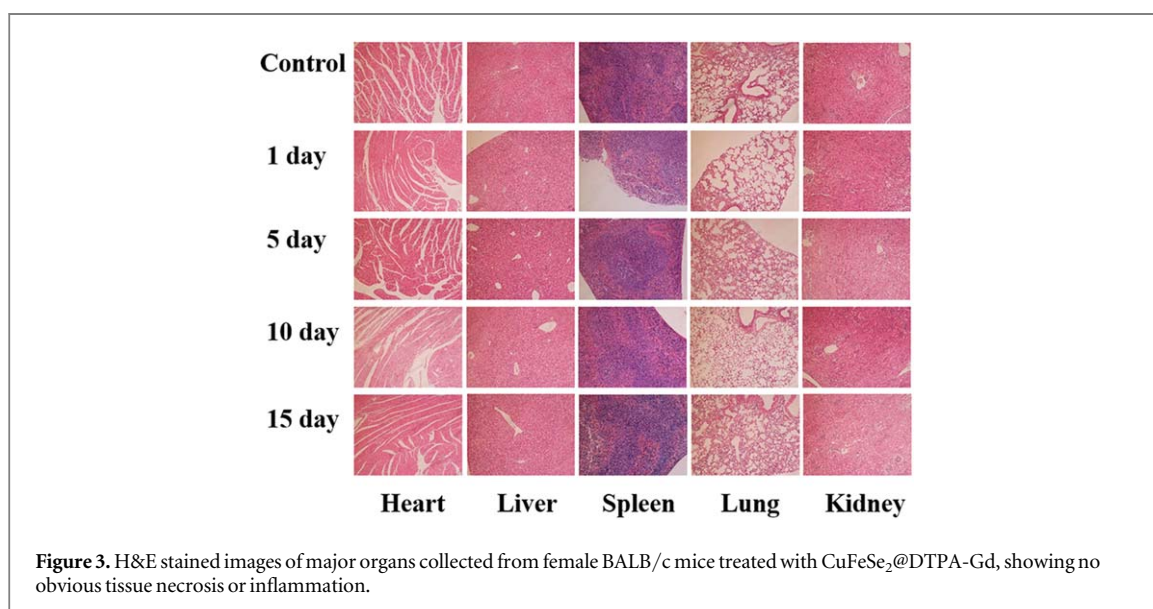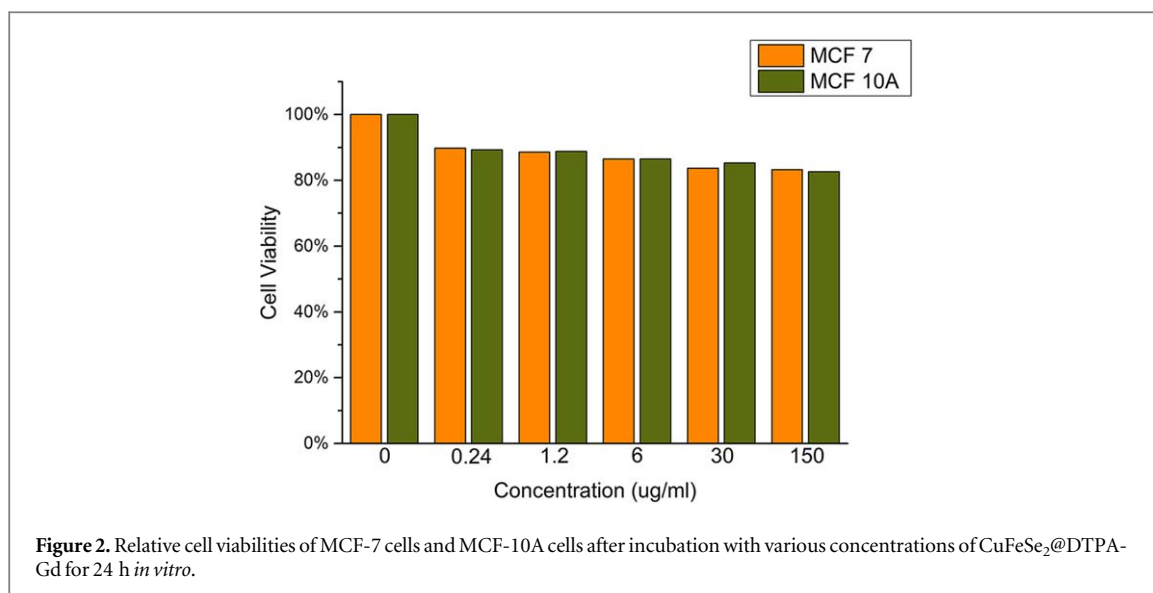
3.2. Biocompatibility

The contrast agent used in clinic should first have well biocompatibility [26]. In this study, the potential cytotoxicity of CuFeSe$_2$@DTPA-Gd was first assessed by standard MTT assay with human breast cancer cells MCF7 and human normal breast cells MCF10A. As shown in figure 2, the survival rates of MCF7 cells and
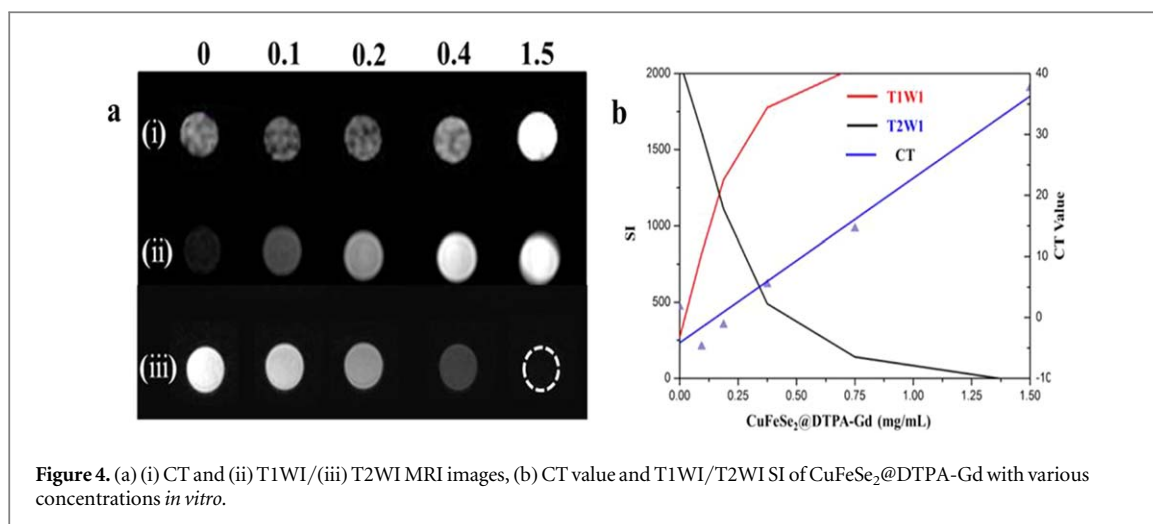
Figure 1. (a), (b) TEM images of CuFeSe$_2$@DTPA-Gd nanocrystals, showing the average particle size of CuFeSe$_2$@DTPA-Gd NCs was 2.47 ± 0.67 nm, (c) particle size distribution of CuFeSe$_2$@DTPA-Gd nanocrystals, counted from 182 nanocrystals shown in typical TEM images, showing these nanoparticles were with small size and their particle sizes were relatively uniform, (d) infrared spectrum results of CuFeSe$_2$@DTPA-Gd, showing surface functional groups of nanoparticles, (e) XRD patterns of CuFeSe$_2$, CuFeSe$_2$@DTPA and CuFeSe$_2$@DTPA-Gd, (f) Magnetization curve of CuFeSe$_2$ and CuFeSe$_2$@DTPA-Gd, identifying the potential of MRI imaging of CuFeSe$_2$@DTPA-Gd nano-contrast agent.

MCF10A cells were over 80% after co-incubation with CuFeSe$_2$@DTPA-Gd (0–150 ug ml^{-1}) for 24 h. This demonstrated that the nanocrystals show no significant cytotoxicity to MCF7 cells and MCF10A cells. We further tested the toxicity of CuFeSe$_2$@DTPA-Gd *in vivo* and evaluated its biological application potential. BABL/C female mice were sacrificed at different time periods after the CuFeSe$_2$@DTPA-Gd injected into the veins of the mice and their main organs (heart, liver, spleen, lung and kidney) were taken for HE staining to evaluate the toxicity of the nanocrystal *in vivo*. It can be observed that treated mice did not show abnormal mental state, diet, weight or death at 1, 5, 10 and 15 days after CuFeSe$_2$@DTPA-Gd injection. In addition, the HE staining results of the treated mice were not significantly different from that of normal mice in the control group, and no tissue necrosis or inflammation was observed (figure 3). These results clearly show that CuFeSe$_2$@DTPA-Gd is less toxic and well biocompatible.

3.3. Imaging capability of CuFeSe$_2$@DTPA-Gd *in vitro*
Then this study used 64 row 128-slice spiral CT scanner and 3.0 T MRI imager to evaluate the imaging performance of CuFeSe$_2$@DTPA-Gd *in vitro*.

Figure 2. Relative cell viabilities of MCF-7 cells and MCF-10A cells after incubation with various concentrations of CuFeSe$_2$@DTPA-Gd for 24 h *in vitro*.

Figure 3. H&E stained images of major organs collected from female BALB/c mice treated with CuFeSe$_2$@DTPA-Gd, showing no obvious tissue necrosis or inflammation.

As shown in figure 4(a) (i), with the increase of the contrast agent concentration, the CT image density of the solution gradually increased, showing a linear relationship between the two (4b). As x-rays pass through different tissues of the body, they attenuate to different degrees, which is the basis for image contrast. Non-enhanced CT is only suitable for different tissues with great difference in density, such as bone and lung. When the CT value between tumor and surrounding soft tissues is similar, it is difficult to form sufficient contrast on the image, and it is easy to miss. In order to solve these problems, various contrast agents have been developed to selectively enhance the image contrast between the target soft tissue and the surrounding tissue to improve CT sensitivity [27]. According to this law that the CT value of CuFeSe$_2$@DTPA-Gd solution linear increased as the concentration increases, this study found that CT value (7412 Hu) of CuFeSe$_2$@DTPA-Gd at 300 mg ml^{-1} was significantly higher than that (5100 Hu) of a clinically commonly used iodine contrast agent (Iopromide), indicating that CuFeSe$_2$@DTPA-Gd can absorb x-rays more effectively and can provide the clinically needed contrast at relatively low concentrations, which can reduce the injection dose and make it have greater potential for clinical application [28, 29]. At the same time, the imaging time of small molecule iodide contrast agent is short, the distribution in the body is non-specific, the osmotic pressure and/or viscosity is high, and the dosage is large, these may cause a strong contrast agent reaction and endanger the patient's life. Compared with traditional small-molecule contrast agents, nanoparticles have longer blood circulation time, lower renal clearance rate and capillary leakage rate, and can be passively accumulated in tumor sites through the high permeability and retention of solid tumors [30].

Figure 4. (a) (i) CT and (ii) T1WI/(iii) T2WI MRI images, (b) CT value and T1WI/T2WI SI of CuFeSe$_2$@DTPA-Gd with various concentrations *in vitro*.

Similarly, the MRI imagings of CuFeSe$_2$@DTPA-Gd nanocrystals solutions *in vitro* with various concentration showed that with the increase of solution concentration, the T1WI signal gradually increased mainly due to the effect of Gd on shortening T1 relaxation time, and at the same time the T2WI signal gradually decreased to disappear mainly due to the ability of CuFeSe$_2$ to shorten transverse relaxation time (figure 4(a) (ii), (iii)). These results confirmed that CuFeSe$_2$@DTPA-Gd can change the relaxation rate of water particles in tissues, thus improving the imaging contrast between different tissues. The above imaging results *in vitro* indicated that the prepared CuFeSe$_2$@DTPA-Gd nano-contrast agent has excellent MRI T1WI/T2WI and CT imaging performance *in vitro*. The study by Jiang *et al* had shown that CuFeSe$_2$, which has a high x-ray attenuation coefficient and superparamagnetism, is an excellent CT/MRI T2WI imaging nano-contrast agent, but lacks T1 imaging capabilities [23]. Although ability of T1WI to detect lesions is not as good as T2WI, it has a relatively high tissue resolution. Therefore, the combination of MRI T1WI and T2WI is conducive to further improve the accuracy of disease diagnosis. Compared with CuFeSe$_2$, CuFeSe$_2$@DTPA-Gd has the additional ability of T1WI imaging, which makes up for the limitations of CT imaging and single T2WI imaging, and further enriches its imaging performance. Magnevist, a commonly used T1-enhanced contrast agent in clinical practice, is the complex of Gd^{3+} and DTPA, which can shorten T1 relaxation time. As a widely used MRI contrast agent, Gd-DTPA has excellent characteristics such as thermodynamic stabilities, kinetic inertnesses, high relaxivities, etc and is usually used to enhance the MRI T1WI signal, especially suitable for tumor MRI enhanced imaging. In this study, by being coupled with CuFeSe$_2$, Gd-DTPA obtained the additional ability to enhance the contrast between tumor and surrounding tissue in MRI T2WI and CT imaging, which is of great significance for early detection of tumor, determination of tumor scope and the determination of therapeutic schedule.

3.4. Multimodal imaging capability *in vivo*

In view of the it's excellent MRI and CT imaging performance *in vitro*, this study then used mice bearing tumors to evaluate the CT and MRI imaging performance of the CuFeSe$_2$@DTPA-Gd *in vivo*. CT images of mice bearing tumor were obtained before and after CuFeSe$_2$@DTPA-Gd (1.5 mg ml^{-1}) intratumorally injected into the tumor. It can be observed that after the injection of the nanoparticle contrast agent, the tumor area's density was increased compared to that obtained before the injection, and the difference of mean CT value of the tumor area before and after the injection of CuFeSe$_2$@DTPA-Gd was statistically significant (P = 0.000) (figure 5 and table 1). This result demonstrated the potential of CuFeSe$_2$@DTPA-Gd in CT imaging. Another group of mice were imaged before and after injection of CuFeSe$_2$@DTPA-Gd into the tumor with a 3.0TMRI scanner, and corresponding MRI images were obtained (figure 5(a)). The results showed that the T1WI signal was increased and the T2WI signal was decreased after the injection of CuFeSe$_2$@DTPA-Gd, and T1WI SICpost/SIMpost was also larger than SICpre/SIMpre (figure 5 and table 1). The differences between the above parameters were statistically significant. This indicated that the nanoparticle CuFeSe$_2$@DTPA-Gd synthesized in this study can also effectively shorten the longitudinal and transverse relaxation time of water particles to achieve MRI T1WI/T2WI dual modal imaging. The above imaging results of CT, MRI *in vitro* and *in vivo* indicated that CuFeSe$_2$@DTPA-Gd has a promising prospect in CT and MRI T1WI/T2WI three-modal imaging.

After reconstructing the original images obtained by IQon CT before and after enhancement into70 Kev virtual monochromatic images, it can be observed that the average CT value of the tumor site after enhancement has changed from 35.7 HU to 84.7 HU (supplementary figure 3(a)).
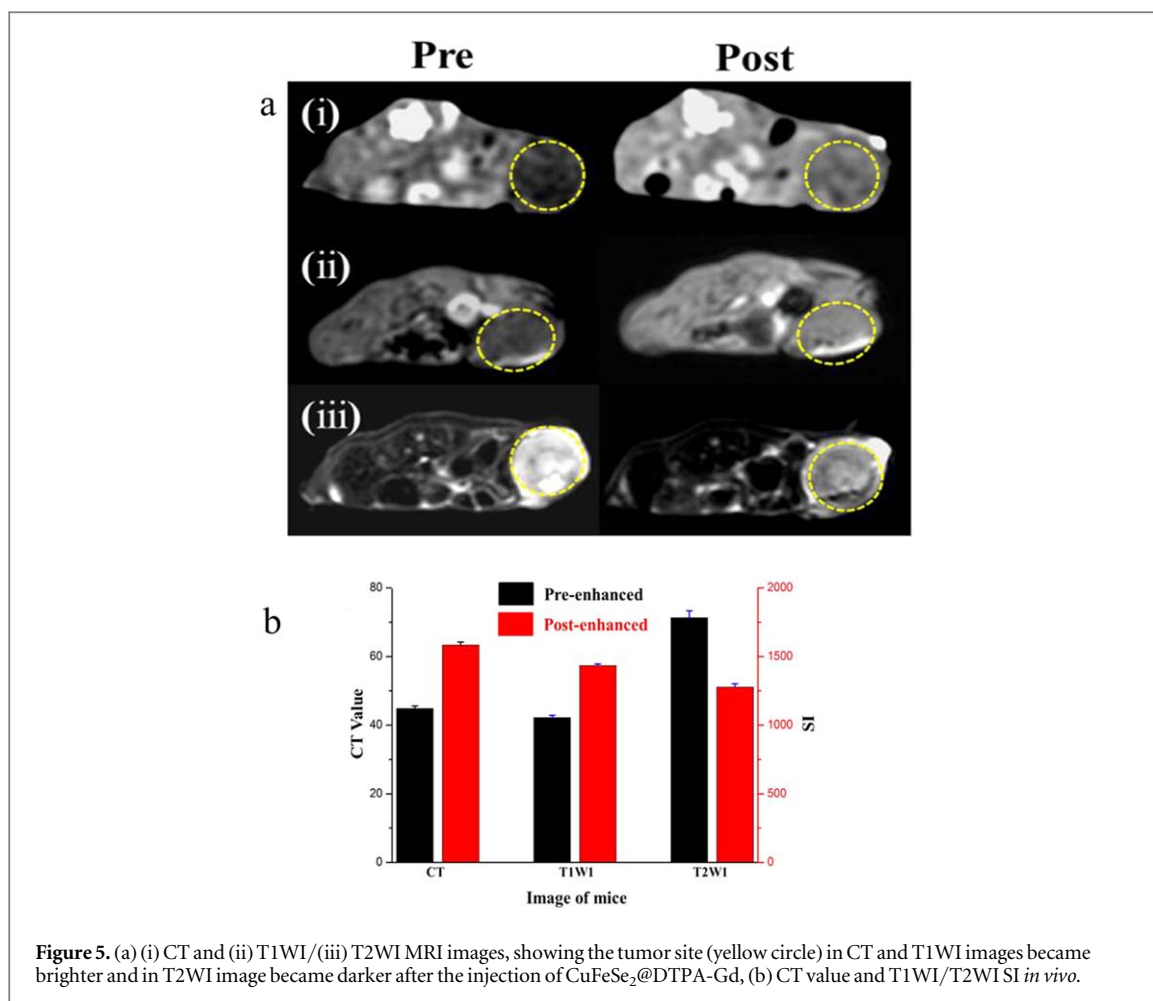
Figure 5. (a) (i) CT and (ii) T1WI/(iii) T2WI MRI images, showing the tumor site (yellow circle) in CT and T1WI images became brighter and in T2WI image became darker after the injection of CuFeSe$_2$@DTPA-Gd, (b) CT value and T1WI/T2WI SI *in vivo*.

Table 1. MRI signal intensity and CT value of tumor obtained pre- and post-intratumoral injection of CuFeSe$_2$@DTPA-Gd.

Group	T1WI SI$_C$	T1WI SI$_C$/SI$_M$	T2WI SI$_C$	T2WI SI$_C$/SI$_M$	CT Value (HU)
Pre-injection (n = 4)	1054.41 ± 16.75	0.91 ± 0.01	1782.50 ± 50.40	8.45 ± 0.37	44.83 ± 0.73
Post-injection (n = 4)	1434.67 ± 11.63	1.27 ± 0.02	1277.16 ± 24.81	6.01 ± 0.28	63.36 ± 0.86
P value	0.001	0.000	0.006	0.003	0.000

$^*P$ value <0.05 is statistically significant.

For T2Map imaging, the average T2Map value of the tumor site changed from 152.67 to 44.91 after enhancement. Similarly, after enhancement, the average T2*map value of the tumor site changed from 23.25 to 3.75 (supplementary figures 3(b) and (c)).

4. Conclusion

In summary, nano-contrast agent CuFeSe$_2$@DTPA-Gd with uniform particle size, good stability, well biocompatibility and multi-functional groups was successfully prepared by simple one-pot method in this study. *In vitro* and *in vivo* studies confirmed that the prepared CuFeSe$_2$@DTPA-Gd possessed desired CT and MRI T1WI/T2WI three-mode imaging properties. In addition, CuFeSe$_2$, as a nanoscale ternary chalcogenides, has high photothermal conversion efficiency and can show an excellent effect on photothermal therapy of cancer. As a multimodal contrast agent, CuFeSe$_2$@DTPA-Gd has a great potential to combine imaging and treatment to realize cancer theranostics. Further MRI/CT imaging-guided photothermal cancer therapy studies of CuFeSe$_2$@DTPA-Gd *in vivo* are currently underway in our group and will be reported in due course.

Acknowledgments

Data availability statement

All data that support the findings of this study are included within the article (and any supplementary files).

Disclosure

On behalf of all authors, the corresponding author states that there is no conflict of interest.

Ethical approval

The animal experiments of this study were carried out in accordance with the principles outlined in the journal's ethical policy and were approved by Experimental Animal Ethics Committee of Southwest Medical University (approval ID: 2020585).

Author contributions

All authors contributed to the study conception and design.

Jian Shu and Lu Yang: Conceptualization, Methodology and Validation.

Lu-Yao Lai, Ying Jiang and Guang-Ping Su: Investigation and Data Curation.

Lu-Yao Lai, Ying Jiang, Shao-Zhi Fu: Project administration.

Lu-Yao Lai, Ying Jiang , Min Wu, Xiao-Fei Lu: Analysis, or interpretation of data.

Lu-Yao Lai and Ying Jiang: Writing - Original Draft.

Jian Shu and Lu Yang: Supervision, Project administration, and Writing—Review & Editing.

ORCID iDs

Jian Shu ⓘ https://orcid.org/0000-0002-7386-7217

References

[1] DeSantis C E, Kramer J L and Jemal A 2017 The burden of rare cancers in the United States *CA Cancer J Clin.* **67** 261–72

[2] Miller K D *et al* 2019 Cancer treatment and survivorship statistics, 2019 *CA Cancer J Clin.* **69** 363–85

[3] Schadendorf D *et al* 2018 Melanoma *Lancet* **392** 971–84

[4] Shapiro C L 2018 Cancer survivorship *N. Engl. J. Med.* **379** 2438–50

[5] Cai X X, Zhu Q X, Zeng Y, Zeng Q, Chen X L and Zhan Y H 2019 Manganese oxide nanoparticles as MRI contrast agents in tumor multimodal imaging and therapy *Int. J. Nanomed.* **14** 8321–44

[6] Herschman H R 2003 Molecular imaging: looking at problems, seeing solutions *Science* **302** 605–8

[7] Weissleder R and Pittet M J 2008 Imaging in the era of molecular oncology *Nature* **452** 580–9

[8] Hussain T and Nguyen Q T 2014 Molecular imaging for cancer diagnosis and surgery *Adv. Drug. Deliv. Rev.* **66** 90–100

[9] James M L and Gambhir S S 2012 A molecular imaging primer: modalities, imaging agents, and applications *Physiol. Rev.* **92** 897–965

[10] Kircher M F and Willmann J K 2012 Molecular body imaging: MR imaging, CT, and US. Part II. Applications *Radiology* **264** 349–68

[11] Key J and Leary J F 2014 Nanoparticles for multimodal *in vivo* imaging in nanomedicine *Int. J. Nanomedicine.* **9** 711–26

[12] Wood C S and Stevens M M 2016 Materials science: improving the image of nanoparticles *Nature* **539** 505–6

[13] Jin D, Xi P, Wang B, Zhang L, Enderlein J and van Oijen A M 2018 Nanoparticles for super-resolution microscopy and single-molecule tracking *Nat. Methods* **15** 415–23

[14] Meng Z, Stolz R M, Mendecki L and Mirica K A 2019 Electrically-transduced chemical sensors based on two-dimensional nanomaterials *Chem. Rev.* **119** 478–598

[15] Mochalin V N, Shenderova O, Ho D and Gogotsi Y 2011 The properties and applications of nanodiamonds *Nat. Nanotechnol.* **7** 11–23

[16] Pelaz B *et al* 2017 Diverse applications of nanomedicine *ACS Nano.* **11** 2313–81

[17] Louie A 2010 Multimodality imaging probes: design and challenges *Chem. Rev.* **110** 3146–95

[18] Lee D E, Koo H, Sun I C, Ryu J H, Kim K and Kwon I C 2012 Multifunctional nanoparticles for multimodal imaging and theragnosis *Chem. Soc. Rev.* **41** 2656–72

[19] Xing Y, Zhao J, Conti P S and Chen K 2014 Radiolabeled nanoparticles for multimodality tumor imaging *Theranostics.* **4** 290–306

[20] Liang G and Xiao L 2017 Gd(3+)-functionalized gold nanoclusters for fluorescence-magnetic resonance bimodal imaging *Biomater. Sci.* **5** 2122–30

[21] Prabhu P and Patravale V 2012 The upcoming field of theranostic nanomedicine: an overview *J. Biomed. Nanotechnol.* **8** 859–82

[22] Jaison D, Meher Abhinav E, Gangwar A, Kishore P N, Chandrasekaran G and Mothilal M 2020 Effect of Gd^{3+} substitution on proton relaxation and magnetic hyperthermia efficiency of cobalt ferrite nanoparticles *Mater. Res. Express* **7** 064009

[23] Jiang X *et al* 2017 Ultrasmall magnetic $CuFeSe_2$ ternary nanocrystals for multimodal imaging guided photothermal therapy of cancer *ACS Nano.* **11** 5633–45

[24] Wang W, Jiang J, Ding T, Wang C, Zuo J and Yang Q 2015 Alternative synthesis of $CuFeSe_2$ nanocrystals with magnetic and photoelectric properties *ACS Appl. Mater. Interfaces* **7** 2235–41

[25] Arami H, Khandhar A, Liggitt D and Krishnan K M 2015 *In vivo* delivery, pharmacokinetics, biodistribution and toxicity of iron oxide nanoparticles *Chem. Soc. Rev.* **44** 8576–607

[26] Ju K Y *et al* 2013 Bio-inspired, melanin-like nanoparticles as a highly efficient contrast agent for T-1-weighted magnetic resonance imaging *Biomacromolecules.* **14** 3491–7

[27] Wathen C A *et al* 2013 *In vivo* x-ray computed tomographic imaging of soft tissue with native, intravenous, or oral contrast *Sensors (Basel)* **13** 6957–80

[28] Rabin O, Manuel Perez J, Grimm J, Wojtkiewicz G and Weissleder R 2006 An x-ray computed tomography imaging agent based on long-circulating bismuth sulphide nanoparticles *Nat. Mater.* **5** 118–22

[29] Wu B *et al* 2018 Gadolinium-chelate functionalized bismuth nanotheranostic agent for *in vivo* MRI/CT/PAI imaging-guided photothermal cancer therapy *Biomaterials* **159** 37–47

[30] Folkman J 1995 Angiogenesis in cancer, vascular, rheumatoid and other disease *Nat. Med.* **1** 27–31